INTERFACIAL AREA TRANSPORT OF STEAM-WATER TWO-PHASE FLOW IN A VERTICAL ANNULUS AT ELEVATED PRESSURES DURING SUB-COOLED BOILING

B. Ozar^{1,2}, C. S. Brooks¹, T. Hibiki¹ and M. Ishii¹

¹ School of Nuclear Engineering, Purdue University, Indiana, USA
² Present address: Fauske and Associates, LLC, Illinois, USA

ozar@fauske.com, csbrooks@purdue.edu, hibiki@purdue.edu, ishii@purdue.edu

Abstract

The interfacial area transport of steam-water two-phase flow in a vertical annulus has been investigated experimentally and theoretically for elevated pressures (a maximum of 1 MPa) during sub-cooled boiling. The modeling of interfacial area transport equation with phase change terms was introduced and discussed along with experimental results. The interfacial area transport equation considered the effects of bubble interaction mechanisms such as bubble break-up and coalescence, as well as, effects of phase change mechanisms such as wall nucleation and condensation for sub-cooled boiling. The benchmark focused on the sensitivity analysis of the constitutive relations that describe the phase change mechanisms.

Keywords: Thermal-hydraulics, bubble, interfacial area, multi-phase flow, void fraction.

Introduction

In the current thermal-hydraulic system analysis code, the interfacial area concentration is calculated with the flow regime-dependent correlations that do not dynamically represent the changes in interfacial structure. The flow regime maps are based on the assumptions of steady-state and fully developed flows. These flow regime maps produce discontinuous changes in the interfacial transfer because very small changes in the state space can lead to a very different steady-state flow regime. To better characterize the effects of interfacial structure and regime transition, a mathematical model which can take into account the dynamic change of the interfacial structure is needed. The formulation of interfacial area transport equations (IATE) is based on statistical mechanics and its concept has been fully established (Ishii and Hibiki [1]). However, the source and sink terms of interfacial area due to bubble coalescence and breakup are still being developed. These are strongly dependent on flow conditions and geometries. So far, most of the interfacial area research has been performed for round tubes and adiabatic flow (Hibiki and Ishii [2]).

A detailed literature review of studies for two-phase flow with phase change is provided by Hibiki and Ishii [2]. The literature review showed that most of these studies were related to measurement of area or volume averaged void fraction or pressure drop in boiling flow. The local measurements of two-phase flow parameters such as void fraction, bubble interface velocity and interfacial area concentration are sorely lacking. Most of the database is limited to area or line averaged void fraction. Furthermore, the principles for modeling phase-change terms are limited to bubbly condensing flows (Hibiki and Ishii [2]).

In this work, the interfacial area transport of vertical, upward, steam-water two-phase flows with phase change in an annular channel have been investigated. Typical data from the fifty seven inlet flow conditions, which covered different system pressures, inlet sub-cooling, inlet liquid velocity and wall heat flux is discussed. The modeling of interfacial area transport equation with phase change terms was also introduced and discussed. The interfacial area transport equation considered the effects of bubble interaction mechanisms such as bubble break-up and bubble coalescence. It also took into account the effects of phase change mechanisms such as wall nucleation and condensation for sub-cooled boiling.

1. Experimental Facility and Instrumentation

The annular test section of the facility was a scaled prototypic boiling water nuclear reactor based on geometric and thermal-hydraulic similarities. Figure 1 shows the schematic of the experimental facility. Differential pressure is measured between the inlet and any of the five measurement points in the test section. The test section was composed of an injection port, five instrumentation ports (z/D_h=52, 149, 108, 189 and 230), a cartridge heater and Pyrex® or stainless steel pipe. The flow channel was an annulus with an inner diameter of 19.1 mm and an outer diameter of 38.1 mm. This annulus was formed between the pipes and the cartridge heater. Pyrex® pipes were used for pressures up to 350 kPa in order to enable flow visualization. However, for pressures above 350 kPa, stainless steel pipes of the same dimensions were used. The test section had a 2845 mm heated section followed by a 1632 mm unheated section where the third port was positioned at the heated-unheated boundary. The function of the unheated section was to observe the condensation of the bubbles, when the flow was still sub-cooled at the end of the heated section. The heater rod was capable of producing a maximum heat flux of 260 kW/m². It also accommodated five thermocouples, which were embedded on the heater surface. These thermocouples were located at the same axial locations as the instrumentation ports and provided wall surface temperature of the heater rod.

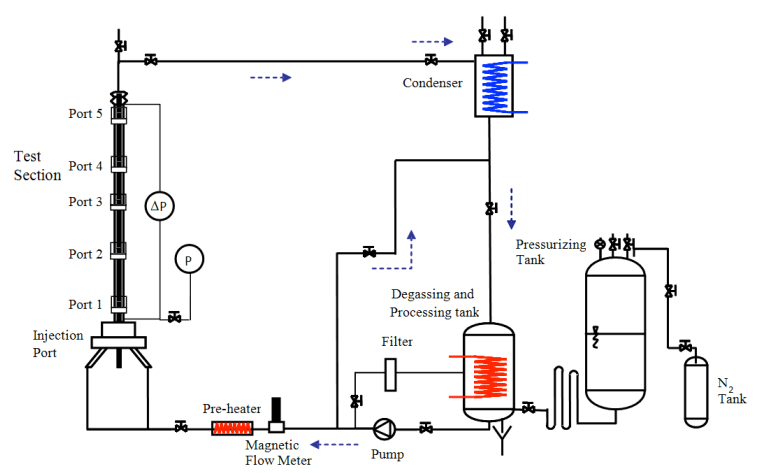


Figure 1 Schematic of the experimental facility

Detailed information of the two-phase flow parameters such as void fraction, bubble velocity and interfacial area concentration as well as the local pressure and temperature, was obtained by the

instrumentation ports. The local void fraction, bubble velocity and interfacial area concentration were measured with a four sensor conductivity probe technique. For the conductivity probe signal processing of the present study, bubbles were divided into two groups; spherical and distorted bubbles as Group-1, whereas cap, slug, and churn-turbulent bubbles as Group-2. This categorization was required since Group-1 and Group-2 bubbles behaved differently and had different contributions to interfacial area concentration. The boundary between the two groups was determined by the maximum distorted bubble diameter in a small gap.

2. Discussion of Experimental Data

Fifty seven inlet flow conditions were conducted and dictated by inlet pressure, inlet liquid velocity, sub-cooling temperature of the liquid at the inlet and the wall heat flux. The inlet pressure ranged from 200 kPa to 950 kPa during the experiments. The inlet liquid velocities varied from 0.24 m/s to 2.6 m/s while the inlet sub-cooling was in the range between 7°C and 30°C. The heat flux was changed between 61 kW/m² and 260 kW/m². The flow conditions generated due to these experimental parameters covered flow regimes including bubbly, capbubbly and churn-turbulent flow. The experimental conditions were representative of operating conditions of a typical boiling water reactor and this was justified by geometrical, hydrodynamic and thermal scaling. In what follows, detailed interpretation of an experimental condition is provided. The selected condition is also the key focus of model benchmarking, which is discussed in a following section.

2.1 Local Flow Structure

The local flow structure is mainly determined by heated/unheated region, sub-cooled bulk liquid, bubble coalescence and breakup. The mechanism of bubble interactions can be summarized in five categories (Ishii and Hibiki [1]): the coalescence due to random collisions driven by liquid turbulence; the coalescence due to wake entrainment, the breakup due to the impact of turbulent eddies, the shearing-off of small bubbles from cap/slug bubbles; and the breakup of large cap bubbles due to surface instability. Also, the mechanisms for thermal effects can be summarized as wall nucleation, bulk evaporation, flashing and bulk condensation. Relative importance of these terms depends on flow conditions.

The radial migration of bubbles also plays an important role in the evolution of local flow structure. Small bubbles tend to move toward the wall by the lift force (and the wall force), whereas large bubbles move toward the center of the channel, resulting in the radial separation of small and large bubbles. This again affects the bubble interactions because they are radially non-uniform but more active near the wall due to the higher turbulent intensity.

Figure 2 presents the local flow measurements for a prototypic condition. The heated section spans until $z/D_h = 148.8$. The unheated section is located downstream of this point. In the heated sub-cooled region, the void fraction demonstrates a sharp peak near the heater wall in a bubble layer region. This can be particularly observed only if the fraction of Group-2 bubbles is not dominant over Group-1 bubbles and the bulk liquid is sub-cooled. The main reason for this

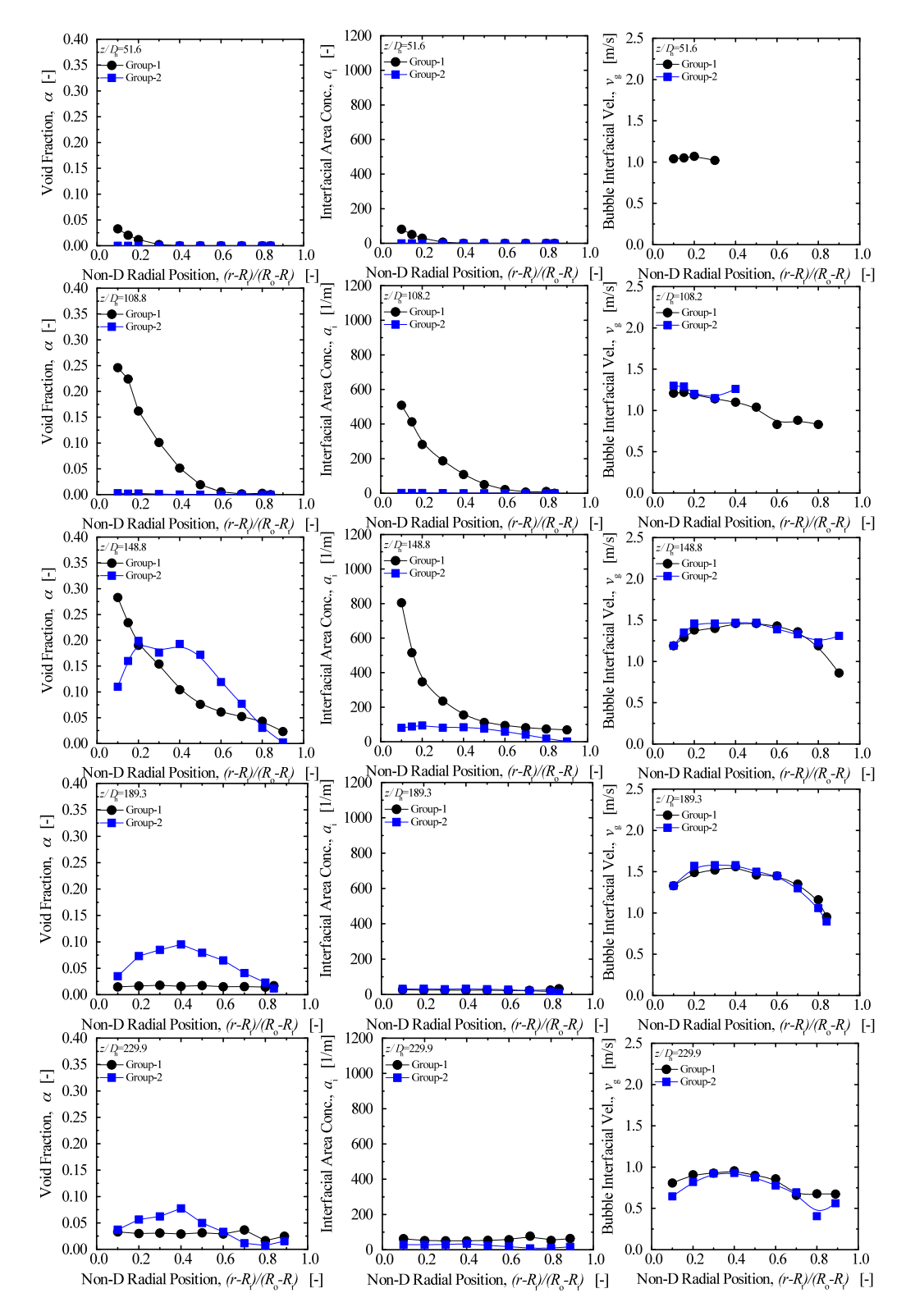


Figure 2 Local void fraction, interfacial area concentration and interface velocity measurements for $q''_w = 241 \text{ kW/m}^2$, $v_{f,in} = 1.02 \text{ m/s}$, $\Delta T_{sub,in} = 14.9 \text{ °C}$ and $P_{in} = 504 \text{ kPa}$

profile is the fact that the bubbles are generated on the heated wall. Then, bubbles condense and collapse further away from the heated wall. However, if the heat flux is sufficient and the bulk liquid is slightly sub-cooled (1~2 °C) or saturated, bubble generation rate increases and Group-2 bubbles form. This is mainly due to two reasons. Firstly, the population of vapor bubbles is high enough to coalesce and form Group-2 bubbles. Secondly, as some bubbles become sufficiently large, they move toward the center of the annulus gap. One side of these large bubbles is adjacent to the super-heated liquid near the heated wall and the other side facing the slightly sub-cooled liquid. The existence and survival of such a bubble depends on the heat balance between the heat received from the super-heated liquid and the heat ejected into the sub-cooled liquid. Once the amount of heat received exceeds the ejected heat, the condition for survival is achieved. Theory, which is discussed in a following section, shows that this is possible when the sub-cooling of the bulk liquid is very low. The wall peaking diminishes as small bubbles get spread in the wake of large bubbles. Therefore, the radial distribution of the void fraction profiles becomes similar to cap-turbulent or churn-turbulent flow profiles of air-water flow.

The last measurement port on the heated section (z/D_h = 148.8) provides the inlet boundary condition to the unheated section since it is located right on the boundary of the heated to unheated section. The two-phase flow structure rapidly transforms from wall-peaked profile to the profiles observed in the adiabatic air-water flow conditions in the unheated section. The lift and wall forces are the major mechanisms. The small bubbles tend to move toward the wall whereas, the larger bubbles toward the center. The bubble interface velocity behaviors for Group-1 and Group-2 bubbles are comparable to the turbulent liquid velocity profiles. The profiles reach a maximum around $(r-R_i)/(R_o-R_i)=0.4\sim0.45$. This is expected since the turbulent liquid velocity profile in an annulus has maxima, which is slightly shifted toward the inner wall. In addition, this shift becomes more distinctive if wall-peaked void fraction profile is observed. This is related with the increased bubble density in this area, thus higher water and vapor velocities.

2.2 Area-Averaged Flow Structure and Axial Evolution of Two-phase Flow Parameters

The axial distributions of area-averaged IAC profiles are presented in Figure 3 for the same experimental condition discussed above. In general, Group 1 bubbles dominate the overall IAC. The axial profiles of area averaged values also looks very similar to the void fraction profile when only Group 1 bubbles exist. However in some cases, once Group 2 bubbles are formed, the IAC decreases significantly even though the flow is in the heated region. The IAC values are also affected by the condensation and flashing mechanisms. In the unheated region, IAC decreases when the bulk liquid is sub-cooled. In contrast, increase in IAC is observed with the flashing phenomenon. However, this increase does not have a sharp gradient similar to the increase in the void fraction values. When flashing occurs, either Group 1 bubbles evaporate to form into Group 2 bubbles or the existing Group 2 bubbles grow bigger. Also, some of the Group 1 bubbles coalesce with the growing Group 2 bubbles. Therefore, some of the Group 1 bubbles are lost in this process and the drastic increase in IAC is suppressed.

If the heat flux in the heated section is increased, the void generation also increases. Thus this results in higher void fractions. Also, Group-1 bubbles may coalesce and form into Group-2 bubbles if the void fraction is sufficiently large enough and the required thermal conditions are achieved as discussed in the previous section. Also, increased heat flux has the effect of increasing the bulk liquid temperature much quicker. Therefore, bulk liquid temperature can reach to saturation conditions in the unheated section for $q'' = 241 \text{ kW/m}^2$ and bulk evaporation/flashing is observed between $z/D_h=189.3$ and 229.9. However, for low heat flux the bulk liquid can still be sub-cooled and nearly all the vapor bubbles generated in the heated section condenses and collapses.

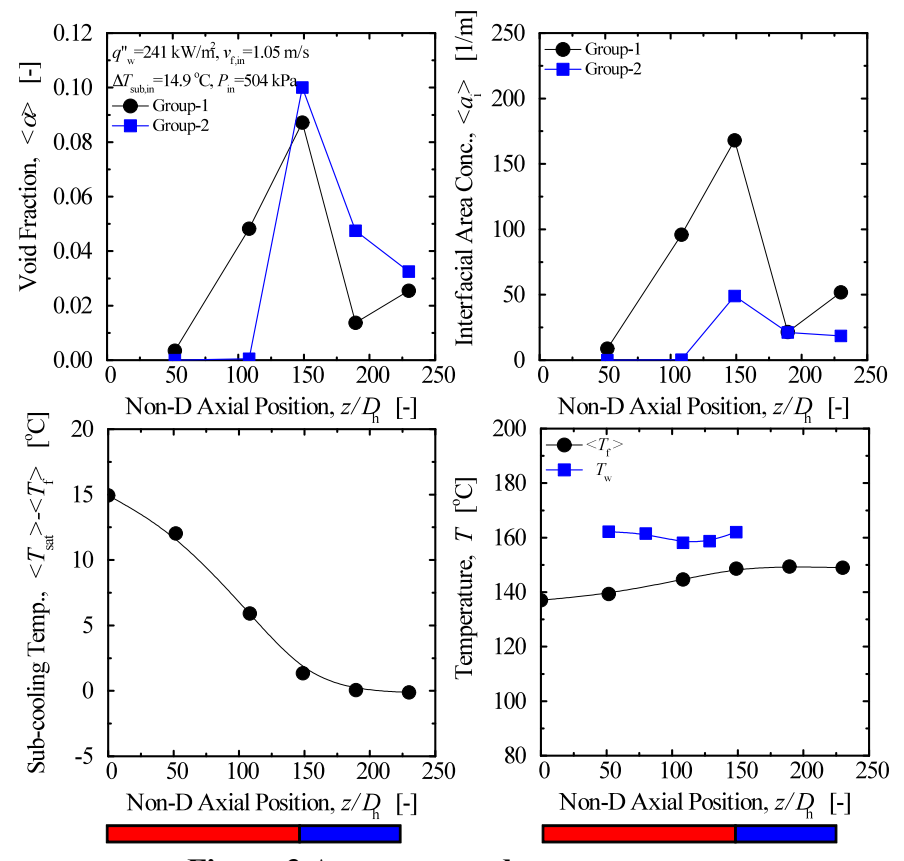


Figure 3 Area-averaged measurements

3. Modeling of Interfacial Area Transport Equation

3.1 Interfacial Area Transport Equation

Ishii and Hibiki [1] thoroughly describe the Two-group Interfacial Area Transport Equations. The phase distribution pattern may not be assumed to be uniform for sub-cooled boiling flow, resulting in large covariances in the 1-D IATE. Therefore, it was proposed that Group-1 bubbles can be averaged within a bubble layer instead of the entire cross section of the flow channel. On the other hand, Group-2 bubbles span all the way across the channel. Thus, the transport equation for these bubbles should be averaged across the whole flow channel area. In the light of this discussion the 1-D transport equations can be given as:

$$\frac{d}{dz} \left(\left\langle a_{i,1} \right\rangle_{B} \left\langle \left\langle \bar{v}_{gz,1} \right\rangle \right\rangle_{B} \right) = \left(\frac{2}{3} - CD_{c1}^{*2} \right) \frac{a_{i,1}}{\alpha_{1}} \left[\frac{d}{dz} \left(\left\langle \alpha_{1} \right\rangle_{B} \left\langle \left\langle \bar{v}_{gz,1} \right\rangle \right\rangle_{B} \right) - \left\langle \eta_{ph1} \right\rangle_{B} \right]
+ \sum_{i} \left\langle \phi_{j,1} \right\rangle_{B} + \left\langle \phi_{ph1} \right\rangle_{B}$$
(1)

$$\frac{d}{dz} \left(\langle a_{i,2} \rangle \langle \langle v_{gz,2} \rangle \rangle \right) = \kappa \frac{\langle a_{i,2} \rangle}{\langle \alpha_2 \rangle} \left[\frac{d}{dz} \left(\langle \alpha_2 \rangle \langle \langle v_{gz,2} \rangle \rangle \right) - \langle \eta_{ph2} \rangle \right]
+ C D_{c1}^{*2} \frac{\langle a_{i,1} \rangle}{\langle \alpha_1 \rangle} \left[\frac{d}{dz} \left(\langle \alpha_1 \rangle \langle \langle v_{gz,1} \rangle \rangle \right) - \langle \eta_{ph1} \rangle \right] + \sum_{i} \langle \phi_{j2} \rangle + \langle \phi_{ph2} \rangle$$
(2)

Here, subscript *B* represents averaging over the bubble layer. The detailed formulation of bubble layer thickness and nomenclature are discussed and provided by Ishii and Hibiki [1].

3.2 Wall Nucleation

The wall nucleation source term, if averaged over the bubble layer area, it can be given as:

$$\langle \phi_{WN} \rangle_B = \frac{\xi_h}{A_B} N_a f_{dp} \pi D_{dp}^2 \tag{3}$$

where ξ_h , A_B , N_a , f_{dp} , and D_{dp} are the heated perimeter, cross-sectional area of the bubble layer, active nucleation site density, bubble departure frequency and bubble departure diameter, respectively. Eq. (3) is valid only when Group-1 bubbles exist. However, Group-2 bubbles may become in contact with the heater rod surface if they exist. In that case, it is assumed that Group-1 bubbles do not nucleate from the section of the heater surface, which is occupied by Group-2 bubbles. Also, it is postulated that all the wall heat flux, where the wall is occupied by Group-2 bubbles, contributes to the evaporation of the super-heated liquid. This results in the growth of Group-2 bubbles. Therefore, this effect should be taken into account. Using,

$$A_{i,2side} = 0.38R_{in}^2$$
, and (4)

$$R_{in} = R - \frac{G}{2}\sin\left(\pi/4\right),\tag{5}$$

where $A_{i,2side}$ and R and are the inner surface area and the radius of curvature of a cap bubble, respectively. G represents the gap in the annulus. And considering bubble shape assumptions, one can obtain

$$p_{\text{exp,2}} = \frac{\langle \alpha_2 \rangle A_c}{\xi_H G} \frac{R_{in}^2}{R^2} \tag{6}$$

to define the ratio of the heat that is transferred to the Group-2 bubbles as the ratio of the side area of the bubble to the total heater area in within a control volume. This term can be multiplied with a factor $C_{W,EXP}$ to take into account the waviness of the bubble surface, and distortions of bubble shape compared to the hypothetical assumption. The interfacial area source for Group-1 wall nucleation resulting from wall nucleation needs to be scaled with the area, which is not occupied by Group-2 bubbles. Thus, Eq. (3) is given after this modification as

$$<\phi_{WN}>_{B} = (1 - p_{\exp,2}) \frac{\xi_{h}}{A_{R}} N_{a} f_{dp} \pi D_{dp}^{2}$$
 (7)

3.3 Condensation

Park et al. [4] described the typical variation of the bubble size during the boiling and condensation process. A bubble first nucleates on a heater surface and rapidly grows (inertia controlled region). The growth rate slows down as the bubble diameter increases and the bubble continues to grow until it reaches to a maximum diameter and it departs from the heater surface (thermally controlled region). When the bubble mixes with the bulk liquid it starts condensing. At low sub-cooling temperature the bubble condensation is controlled by heat transfer. However, when the bubble reaches to a critical size, it can not sustain anymore and collapses suddenly. Park et al. [4] modeled the loss of interfacial area in the heat transfer controlled region, ϕ_{PC} , and the inertia controlled region, ϕ_{CO} .

$$\phi_{PC} = -4\pi \cdot (1 - p_c) \cdot \psi \cdot \frac{a_i^3}{\alpha^2} \cdot Nu_c \cdot J\alpha \alpha_f, \text{ and}$$
(8)

$$\phi_{CO} = R_{ph} \cdot \pi D_b^2 = -\pi D_b^2 \cdot \psi \cdot \frac{a_i^3}{\alpha^2} \cdot \frac{1}{t_c}$$
(9)

where, Nu_c , Ja, α_f , ψ and t_c are defined as the condensation Nusselt number, Jacob number, thermal diffusivity, the factor depending on the shape of the bubbles and the residence time of the bubbles in the heat transfer controlled region, respectively. p_c and D_b are the fraction of bubbles in the inertia-controlled region and the bubble diameter at the region boundary, respectively. D_b is derived based on force balance and Classius Clapeyron approximation and p_c is based on the residence time when the bubbles remain in the heat transfer controlled region. Details of the derivations are provided by Park et al. [4].

Eqs. (8) and (9) can be written in the form of bubble layer averaged terms as the following:

$$\left\langle \phi_{PC,1} \right\rangle_{B} = -4\pi \cdot (1 - p_{c}) \cdot \psi \cdot \frac{\left\langle a_{i,1} \right\rangle_{B}^{3}}{\left\langle \alpha_{1} \right\rangle_{B}^{2}} \cdot Nu_{c} \cdot J\alpha \alpha_{f}, \text{ and}$$
 (10)

$$\left\langle \phi_{CO,1} \right\rangle_{B} = R_{ph} \cdot \pi D_{b}^{2} = -\pi D_{b}^{2} \cdot \psi \cdot \frac{\left\langle a_{i,1} \right\rangle_{B}^{3}}{\left\langle \alpha_{1} \right\rangle_{B}^{2}} \cdot \frac{1}{t_{c}}$$

$$(11)$$

This model was for bulk condensation of spherical bubbles and it was assumed that the bubbles completely mixed with the bulk liquid. The driving force for the bulk condensation mechanism was the temperature difference between the gas space temperature inside the bubble and the bulk liquid temperature.

The condensation mechanism for Group-2 bubbles are modeled in a similar way in this work. Group-2 bubbles are always assumed to be in the thermally controlled region. The condensation term for these should be taken into account when their size is bigger than the critical bubble diameter. If we assume that the Sauter mean diameter scales the size of the bubble, the probability (p_2) of a bubble being larger than the critical bubble diameter can be estimated. Finally, the interfacial area concentration sink term of Group-2 bubbles due to thermal controlled region can be derived (Ozar [5]),

$$\phi_{PC,2} = -p_2 \psi_2 \frac{a_{i2}^3}{\alpha_2^2} \frac{h_{c2} \left(1.52R + 3.28G\right) \left(0.76R^2 + 3.28RG\right)}{0.76\rho_g i_{fg} RG} (T_{sat} - T_f). \tag{12}$$

However, this model can not be solely used during the sub-cooled boiling conditions when the majority of bubbles do not span across the whole channel gap. In that case, most of the bubbles are close to the heated wall, where the effective sub-cooling is less than the one in the bulk flow. TRAC-P [6] uses an additional model to account for the condensation of vapor bubbles near the heater surface. It is assumed that a known amount of heat flux, wall condensation heat flux, is removed from the bubble layer. The wall condensation heat flux model is given as

$$q_{CON,w}'' = 0.075 \frac{D_h}{4} i_{fg} \frac{\rho_f \rho_g}{\rho_f - \rho_g} \alpha \left(T_{sat} - T_f \right)$$

$$\tag{13}$$

TRACE utilizes a weighting method between the condensation near the heated wall and bulk condensation to account for the mass transfer. This relation can be given by,

$$\Gamma_{CON} = \left[\frac{4D_h}{A_c} W_{sub} q_{CON,w}'' + \left(1 - W_{sub} \right) h_c a_i \left(T_{sat} - T_f \right) \right] / i_{fg}$$

$$\tag{14}$$

where W_{sub} is the weighing factor. Considering that this phenomenon can be observed only for Group-1 bubbles and following Park et al.'s [4] formulation by replacing the temperature difference driven interfacial heat flux with a known heat flux, the following can be obtained in the form of bubble layer averaged form.

$$\left\langle \phi_{PC1,w} \right\rangle_{B} = -\left(1 - p_{c,1}\right) \left\langle n_{b,1} \right\rangle_{B} \frac{d\overline{A}_{i,1}}{dt} = -\frac{2}{3} \left(1 - p_{c,1}\right) \frac{q_{CON,w} \cdot \xi_{H}}{A_{B} \cdot \rho_{\sigma} \cdot i_{f,\sigma}} \frac{\left\langle a_{i,1} \right\rangle_{B}}{\left\langle \alpha_{1} \right\rangle_{B}}, \text{ and}$$
(15)

$$\left\langle \phi_{CO,w} \right\rangle_{B} = -\pi D_{b}^{2} \cdot \psi \cdot \frac{\left\langle a_{i,1} \right\rangle_{B}^{3}}{\left\langle \alpha_{1} \right\rangle_{B}^{2}} \cdot \frac{1}{t_{c,w}} \tag{16}$$

It is postulated in this study that the weighting function should be related to the ratio of the area of the bubble layer to the entire channel. This is based on the assumption that the amount of the vapor bubbles condensing in the bubble layer should be proportional to how wide of an area the bubble layer occupies. Therefore the weighting function is provided in the following form

$$W_{sub} = 1 - \frac{A_B}{Ac} \tag{17}$$

Group-2 bubbles span all across the channel and the condensation phenomena is dictated by the bulk condensation mechanism only. Therefore, no weighting function is required. Finally, the condensation sink terms for IATE can be summarized as Group-1

$$\left\langle \phi_{CON,1} \right\rangle_{B} = W_{sub} \left(\left\langle \phi_{CO,w} \right\rangle_{B} + \left\langle \phi_{PC,w} \right\rangle_{B} \right) + (1 - W_{sub}) \left(\left\langle \phi_{CO,1} \right\rangle_{B} + \left\langle \phi_{PC,1} \right\rangle_{B} \right) \tag{18}$$

Group-2

$$\left\langle \phi_{CON,2} \right\rangle = \left\langle \phi_{PC,2} \right\rangle \tag{19}$$

3.4 Model comparison

Interfacial area transport equations for Group-1 and Group-2 bubbles have six unknowns. Additional equations, such as void transport, momentum and energy equations, are needed to close the problem. However, the sole purpose of the comparison is to benchmark the IATE not the entire calculation scheme for predicting two-phase flow behavior. Therefore, in each calculation step of axial direction, $\langle \alpha_1 \rangle$, $\langle v_{gz1} \rangle$, $\langle v_{gz2} \rangle$ bulk liquid temperature, pressure and wall surface temperature are estimated based on measured values and interpolation within between the measurement points; $\langle \alpha_2 \rangle$ is calculated from the inter-group void fraction transport while $\langle \alpha_1 \rangle$ is determined from $\langle \alpha_1 \rangle$ and $\langle \alpha_2 \rangle$. Finally, $\langle a_{i1} \rangle$ and $\langle a_{i2} \rangle$ are calculated based on the corresponding sink/source terms. Also, $\langle \alpha_2 \rangle = 1 \times 10^{-4}$ and $D_{Sm,2} = D_c$ is used as to seed the calculation at $\langle \alpha \rangle = 0.02$. The coefficient C accounts for the effect of the inter-group transport at the group boundary. Currently, a practical method has been implemented to calculate the C value from the bubble number frequency with respect to the bubble chord length, which can be obtained from the conductivity probe measurements for each flow condition. However, the final result is given as

$$C = 4.44 \times 10^{-3} \left(\frac{\langle D_{Sm,1} \rangle}{D_c} \right)^{0.36} \langle \alpha_1 \rangle^{-1.35}$$
 (20)

where $D_c = 1.7 G^{1/3} \left(\sigma/g\Delta\rho \right)^{1/3}$. The bubble interaction mechanisms are calculated by using Sun et al.'s [3] constitutive relations due to an analogy between a rectangular duct and an annulus. The interfacial source and sink terms as well as the mass transfer terms are modeled by using the formulation presented in this work.

The experimental condition described in section 2 is considered for model comparison purposes. The experimental condition calls for a 2-Group IATE calculations in cap-bubbly flow $(q_w'' = 241 \, \mathrm{kW/m^2}, \ v_{f,in} = 1.02 \, \mathrm{m/s}, \ \Delta T_{sub,in} = 14.9 \, ^{\circ}\mathrm{C}$ and $P_{in} = 504 \, \mathrm{kPa}$) under sub-cooled boiling conditions. The results of these calculations are shown in Figure 4. CALC4 presented the most accurate results. Wall nucleation source, expansion and condensation are identified as the major effects for Group-1 bubbles. On the other hand, expansion of Group-2 bubbles through vaporization of the super-heated liquid and expansion of Group-1 bubbles to form Group-2 bubbles have the most dominant effect on Group-2 bubbles. It should be noted that expansion of Group-1 bubbles to form Group-2 bubbles contributes on both the first and second terms on the right hand side of Eq. (2). Also, it is realized that the Group-2 bubbles rapidly grow and expand when the bulk liquid sub-cooling becomes relatively low (approximately less than 2°C downstream of $z/D_h = 100.0$).

CALC5 also shown in Figure 4 is performed in order to demonstrate the importance of the effect of expansion in Group-2 bubbles through the absorption of heat from the super-heated liquid. It is realized that without this term, the amount of Group-2 bubbles generated by the expansion of Group-1 bubbles and bubble interaction mechanisms is insufficient. Although the prediction of

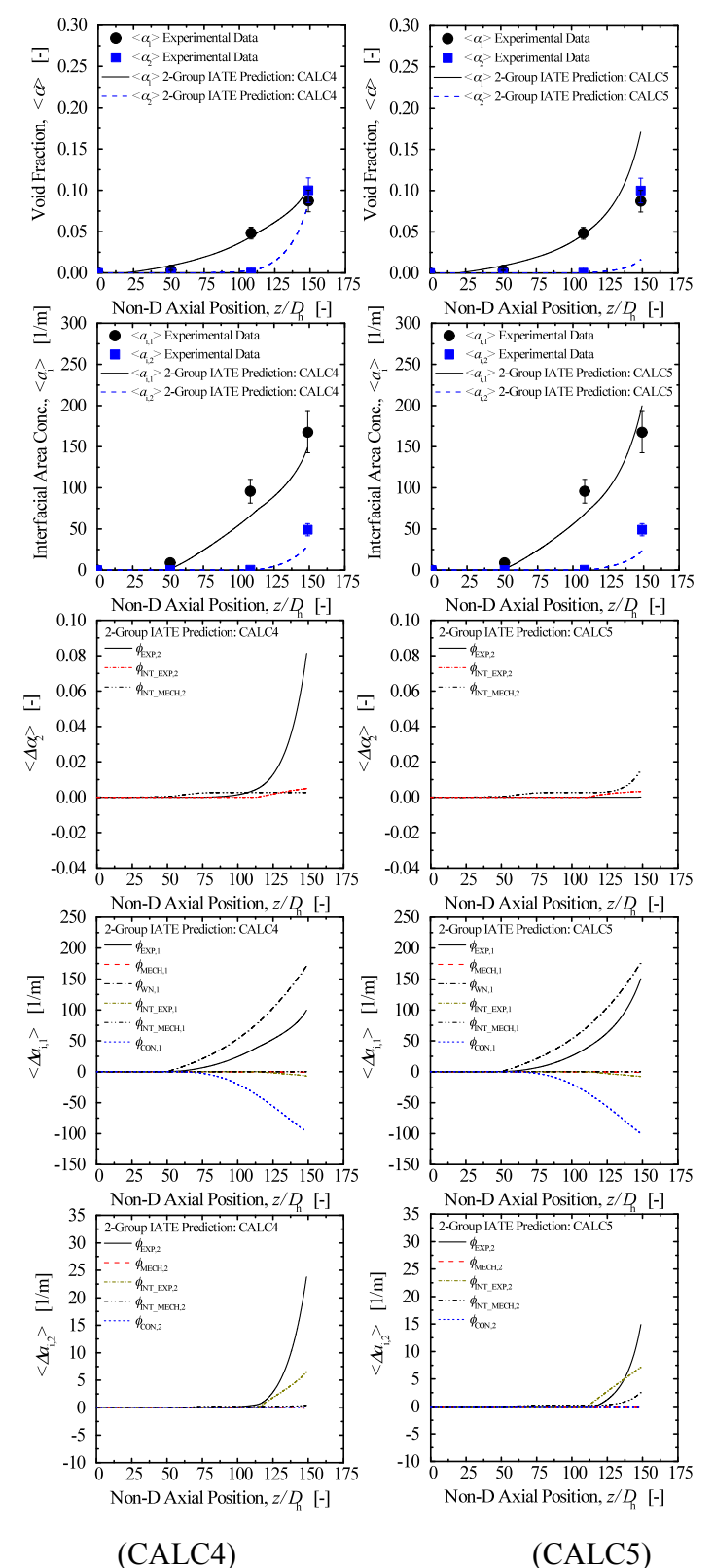


Figure 4 Prediction results of CALC4 and CALC5 with 2-Group IATE

interfacial area concentration is relatively comparable to the previous calculation, this is mostly due to the contribution of the expansion of Group-1 bubbles to form Group-2 bubbles.

4. Conclusions

An experimental study on the interfacial area transport of vertical, upward, steam-water two-phase flows in an annular channel was performed for fifty seven inlet flow conditions at pressures ranging from 200 kPa to 950 kPa. The data includes local multi-group void fraction, interfacial area concentration, and interfacial velocities. IATE modeling and benchmark was performed and the major findings are summarized as follows.

- Sun et al.'s [3] constitutive relations were selected and the parameters in the constitutive relations were averaged either over the bubble layer or the entire flow channel, based on physical considerations.
- The model for bulk condensation sink term of Group-1 bubbles by Park et al. [4] was discussed and utilizing a similar approach to this model, bulk condensation of Group-2 bubbles was modeled. Near wall condensation mechanism was predicted by following an approach, which was similar to Park et al.'s [4]. The total condensation sink term for the interfacial area concentration was assumed to be a combination of these two mechanisms utilizing a weighing factor.
- A new mechanism was suggested for the expansion of Group-2 bubbles which considered the evaporation of the super-heated bulk liquid between the heater surface and the Group-2 bubble interface.
- The wall nucleation, expansion and bulk condensation were identified as the dominant mechanisms for Group-1 bubbles where the wall nucleation source term was the major mechanism controlling the other events.
- The expansion of Group-1 bubbles was the main triggering event for the formation of Group-2 bubbles. Also, the importance of the evaporation of liquid from the super-heated layer for the expansion of Group-2 bubbles was demonstrated.

5. References

- [1] Ishii, M., and Hibiki, T., 2006, "Thermo-fluid dynamics of two-phase flow," Springer, New York, USA.
- [2] Hibiki, T., and Ishii, M., 2009, "Interfacial Area Transport Equations for Gas-Liquid Flow," J. Comp. Multiphase flow, Vol. 1, pp. 1-22.
- [3] Sun, X., Kim, S., Ishii, M., and Beus, S.G., 2004, "Modeling of bubble coalescence and disintegration in confined upward two-phase flow," Nucl. Engr. Des., Vol. 230, pp. 3-26.
- [4] Park, H.S., Lee, T.H., Hibiki, T., Baek, W.P., and Ishii, M, 2007, "Modeling of condensation sink term in the interfacial area transport equation," Int. J. Heat Mass Transfer, Vol. 50, pp. 5041-5053.
- [5] Ozar, B., 2009, "Interfacial area transport of steam-water two-phase flow in a vertical annulus at elevated pressures," Ph.D. Thesis, Purdue University, West Lafayette, IN.
- [6] Spore, J.W., Jolly-Woodruff, S.J., Knight, T.K., Lin, J.C, Nelson, R.A, Pasamehmetoglu, K.O., Steinke, R. G., and Unal, C., 1993, "TRAC-PF1/MOD2 Volume 1:Theory manual," LA-12031-M, Vol. I, NUREG/CR-5673. USA.